Spatially resolved density measurements of singlet delta oxygen in a non-equilibrium atmospheric pressure plasma jet by molecular beam mass spectrometry

Jingkai Jiang¹, Yolanda Aranda Gonzalvo^{1,2} and Peter J. Bruggeman^{1,*}

¹Department of Mechanical Engineering, University of Minnesota, 111 Church Street SE, Minneapolis 55414 Minnesota

²Department of Chemical Engineering and Materials Science, University of Minnesota, 421 Washington Ave. SE, Minneapolis 55455 Minnesota

*email: <u>pbruggem@umn.edu</u>

Abstract

Singlet delta oxygen ($O_2(a^1\Delta_g)$), the first electronically excited state of O_2 , plays an important role in many applications. We report the first measurements of absolute densities of $O_2(a^1\Delta_g)$ in an atmospheric pressure plasma jet (APPJ) by molecular beam mass spectrometry (MBMS). The ability to measure axial and radial profiles of $O_2(a^1\Delta_g)$ impinging on a substrate in the effluent of the APPJ is a key advantage of the MBMS diagnostic method over previously reported optical methods. The measured large $O_2(a^1\Delta_g)$ densities in the APPJ effluent, up to one order of magnitude higher than the O density, underline the potential importance of $O_2(a^1\Delta_g)$ in many applications using APPJs.

Key words: singlet delta oxygen, absolute density, APPJ, molecular beam mass spectrometer

1. Introduction

Singlet oxygen, $O_2(a^1\Delta_g)$, is the first electronically excited state of molecular oxygen with an internal energy of 0.98 eV [1]. It is efficiently produced by electron impact in low-temperature plasmas. Compared with the other electronically excited states of O_2 with higher excitation energies, it has a much longer radiative lifetime (~75 min) and low collisional quenching probabilities enabling high densities of $O_2(a^1\Delta_g)$ in the gas phase plasma [1]. These large $O_2(a^1\Delta_g)$ densities can cause a significant increase in the effective rates of chemical reactions with O_2 in low temperature plasmas.

Many studies have shown the importance of $O_2(a^1\Delta_g)$ in biomedical applications. For example, $O_2(a^1\Delta_g)$ produced by exposing precursor molecules under near-IR light can be the primary active species for the inactivation of cancer cells in photodynamic therapy (PDT) [2]. $O_2(a^1\Delta_g)$ is also suggested to be responsible for the observed selectively of plasma treatment of cancer cells or

tumors [3]. Apart from biomedical applications, the highly reactive properties of $O_2(a^1\Delta_g)$ play a significant role in applications associated with gas-phase chemical reactions such as plasma-assisted combustion. It has been already shown that $O_2(a^1\Delta_g)$ can help to reduce the gas temperature and reduce the delay time required for ignition in H_2 - O_2 combustion [4] by accelerating the oxidation of CH_4 in air [5]. The underlying mechanisms responsible for the beneficial synergistic effects in plasma-catalysis are to date not understood but are typically suggested to be due to the production of reactive species [6] and $O_2(a^1\Delta_g)$ as a likely candidate.

To investigate the role of $O_2(a^1\Delta_g)$ in the plasma processes underpinning the above applications, sensitive diagnostic methods are required to measure the absolute densities of $O_2(a^1\Delta_g)$. Several optical diagnostic methods have been reported in literature including cavity ring-down spectroscopy (CRDS) [7], off-axis integrated-cavity-output spectroscopy (ICOS) [8], radar resonance-enhanced multi-photon ionization (REMPI) [9] and absolute emission spectroscopy [10]–[12]. Absolute densities of $O_2(a^1\Delta_g)$ have been measured for APPJs in open air [13],[14] using infrared optical emission spectroscopy (IOES). A two-dimensional distribution of the $O_2(a^1\Delta_g)$ density was reported in [14] enabling the investigation of the production of $O_2(a^1\Delta_g)$. While this optical diagnostic technique can be performed in-situ, the reported measurements were all performed in the bulk of plasmas or for free jets without substrate and often required the use of an absorption cell. The obtained densities of $O_2(a^1\Delta_g)$ in the free jet cannot directly be extrapolated to the corresponding densities at substrate surfaces including catalysts, liquid or biological samples. In this paper, we address the need to characterize *in-situ* local fluxes of $O_2(a^1\Delta_g)$ impinging on a substrate. Molecular beam mass spectrometer (MBMS) is used to measure the absolute density of $O_2(a^1\Delta_g)$ in the effluent of an RF-driven APPJ as a new approach to enable the measurement of spatially resolved $O_2(a^1\Delta_g)$ densities at substrates.

2. Experimental methods

We used the same MBMS approach which has been used for the detection of radicals and vibrationally excited species: threshold ionization MBMS [15–19]. This approach enables us to exploit the difference between the ionization energy of O_2 (12.1 eV) and $O_2(a^1\Delta_g)$ (11.1 eV). The difference between these two threshold energies enables the distinction of the O_2^+ signal obtained by the MS when the electron energy of the ionization source is sufficiently narrow. Nonetheless, the relatively small energy difference of 0.98 eV makes this a challenging measurement. The MBMS system used in this work is similar to the system described in [20] and is described in detail in [21]. Three pumping stages separated by aligned skimmers are used to reduce the pressure from

the atmospheric environment (760 Torr) to the pressure at which the MS operates (10^{-6} Torr). The diameter of the sampling orifice is chosen to be 30 μ m, smaller than the typical sheath thickness at atmospheric pressure to avoid penetration of the plasma into the first low-pressure stage [22]. The plasma jet used to produce $O_2(a^1\Delta_g)$ was placed in a vacuum chamber mounted on the MBMS flange containing the sampling orifice to provide a highly controlled-gas environment and avoid any fluctuations in the O_2 density in the jet effluent which typically occurs for jets operating with noble gases in an ambient air surrounding. The schematic of the experimental system is shown in Fig. 1.

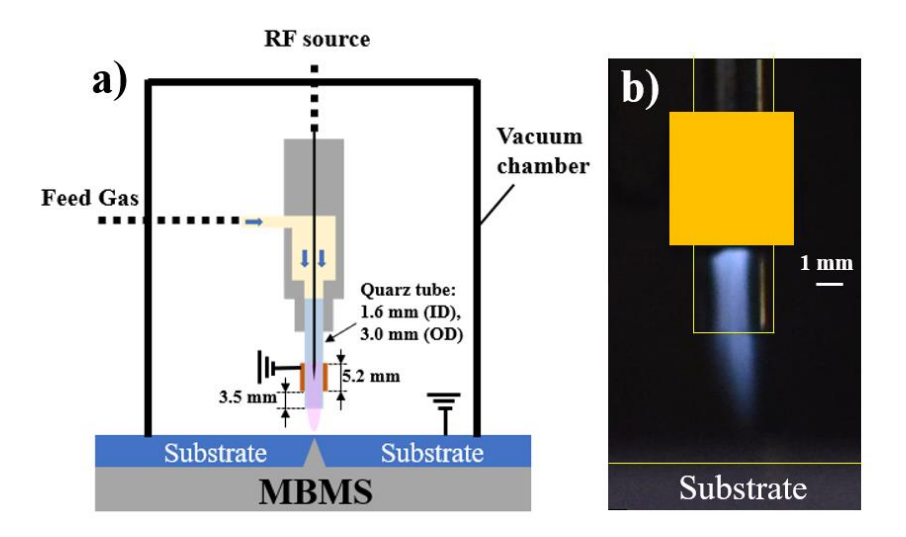


Figure 1. (a) Schematic of the experimental system; (b) image of the plasma jet impinging on the sampling plate of the MBMS at a nozzle-to-substrate distances at 5 mm.

All the experiments in this work were performed in an Ar+1% O_2 environment at atmospheric pressure. The geometry of the jet was identical to the one used in [21] with only one change: the length of the quartz tube is 2.5 mm longer. This enabled to increase the distance between the ground electrode and the nozzle of the quartz tube to 3.5 mm to prevent the formation of a direct discharge between the high voltage needle and the grounded ring electrode in the Ar+1% O_2 environment in the vacuum vessel. The APPJ was driven by a radio frequency (12.1 MHz) sinusoidal wave modulated at a frequency of 40 kHz with a 50% duty cycle (DC). The power absorbed by the plasma during the plasma-on period was kept constant at 10 W (time-averaged power of 5 W) and the feed gas flow rates for argon and oxygen were fixed at 500 sccm and 5 sccm, respectively. The APPJ was mounted on motorized x-y-z translation stages with a spatial resolution of 6 μ m to enable an accurate adjustment of the position of the jet. All the measurements presented in this study were recorded without direct contact of the plasma to the sampling plate as confirmed by time-resolved

power measurements [23]. Indeed, a significant increase in the power was observed, when the plasma coupled to the metal sampling plate. The visible length of the plasma plume was ~ 3 mm as shown in Fig. 1. More detailed information of the MBMS and the APPJ used in this work can be found in [21].

For measuring short-lived neutral species by MBMS, it is necessary to separate the beam component and the background component in the ionizer both contributing to the total signal obtained by the MS. The beam and background components refer to the ions created from the sampled molecular beam entering the ionizer and the ions created from the background gas inside the ionizer, respectively. While most measurements were performed with the original ionizer manufactured by Hiden Analytical Ltd. A modified ionizer with holes on the side wall was used to reduce the background gas inside the ionizer to enable more accurate measurements by beam modulation. Two approaches to substract background signals from the MBMS measurements have been used in this work: modulating the plasma power, already modulated at 40 kHz, at a frequency of 100 Hz with a 50% DC to allow for the convective removal of the plasma-produced species between two plasma cycles; and using a chopper positioned in the second pumping stage of the MBMS system to modulate the molecular beam itself while the plasma is operated without the 100 Hz modulation.

3. Results and discussions

3.1 Identification of $O_2(a^1\Delta_g)$

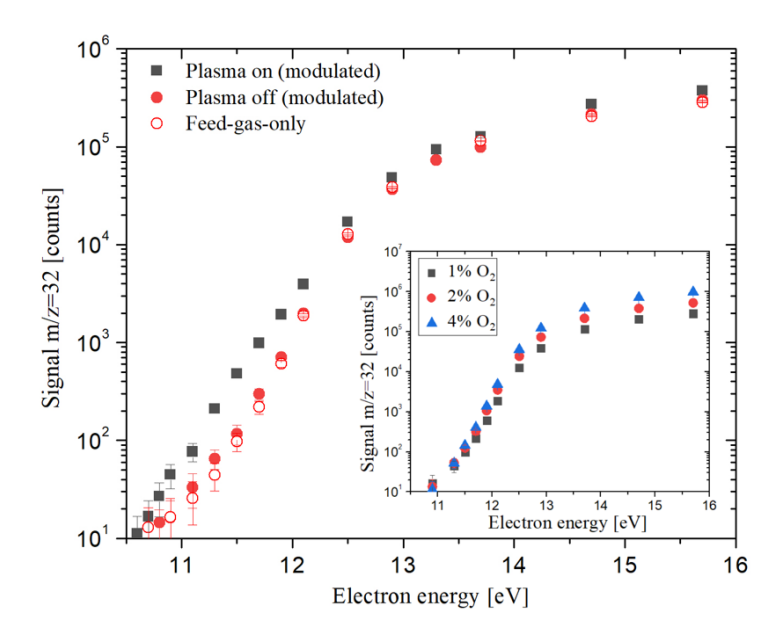


Figure 2. MS signals for O₂⁺ as a function of the electron energy of the ionizer measured at a nozzle-substrate distance of 5 mm. The plasma-on and plasma-off signals represent the total signal and the background signal for the time-resolved measurements recorded during a modulation period, respectively. The feed-gas-only signal is recorded for identical conditions as for the plasma case but without applying the RF power. The recorded electron energy of the ionizer has been shifted so that the measured Ar ionization threshold matched 15.8 eV.

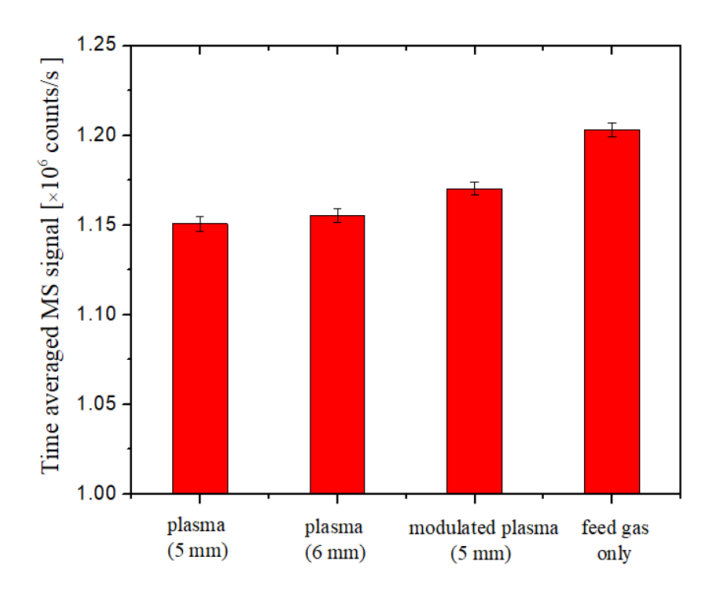


Figure 3. Time-averaged MS signals of Ar for plasma, modulated plasma at 100 Hz and feed-gas-only cases in Ar+1%O₂ as measured with an electron energy of 70 eV in the ionizer.

Fig. 2 shows the MS signals for O_2^+ as a function of the electron energy of the ionizer for the plasma-on, plasma-off and feed-gas-only cases. The highest temperature of the impinging gas measured by reversible temperature indicating labels (OMEGA, RLC-50-30/90) is about 350 \pm 10 K at a nozzle-to-substrate distance of 5 mm. This is an upper estimate of the sampled gas temperature because this measurement was performed with a ceramic substrate having a much lower thermal conductivity than the metal substrate used for the sampling by the MBMS. Furthermore, Fig. 3 shows that the largest difference of the MS signals for Ar⁺ measured at 70 eV for plasma, modulated plasma and feed-gas-on only cases was within 5% (corresponding to a maximum temperature of \sim 315 K) for all plasma conditions used in this study, confirming that the influence of gas temperature can be neglected for the sampled gas. The plasma-off and feed-gas-only signals yield within the experimental accuracy the same result confirming that the plasma does not significantly affect the background O_2 signal. The difference between the plasma-on and plasma-off signals indicates the existence of an excited state of O_2 created by plasma which is

 $O_2(a^1\Delta_g)$ as we will motivate below [24]. The subfigure in Fig. 2 shows the MS signals of O_2^+ as a function of the electron energy for different O_2 concentrations (1%-4%). The corresponding MS signals are similar when the electron energy is below 12 eV, suggesting the contribution is due to a background. This background is observed below the direct ionization potential of ground-state O_2 and might be due to the presence of some $O_2(a^1\Delta_g)$ created by the hot filament of the ionizer in the background gas, or the profile of the energy distribution of the emitted electron beam. Nonetheless, similar measurements have also been performed for Ar to assess the width of the electron energy of the ionizer which was found to be \sim 0.5 eV. This value was obtained by comparing the Ar⁺ signal as a function of ionizer electron energy with the argon ionization cross section convoluted with a Gaussian distribution with different full width at half maxima. The above analysis confirms that the plasma-off signal can be considered as a proper background that is not very sensitive to the O_2 concentration.

The possible contributions to the signal enhancement for the plasma-on case are $O_2(a^1\Delta_g)$, $O_2(b^1\Sigma_g^+)$ and $O_2(v=1-4)$. The lifetimes of $O_2(a^1\Delta_g)$, $O_2(b^1\Sigma_g^+)$ and $O_2(v=1-4)$ are dominated by collisional quenching at atmospheric pressure [25]. The rate coefficients of the dominant quenching reactions are shown in Table 1. The lifetimes of $O_2(a^1\Delta_g)$, $O_2(b^1\Sigma_g^+)$ and $O_2(v=1-4)$ in the effluent of the APPJ can be calculated as:

$$\tau = \frac{1}{k_0 n_0 + k_{0_2} n_{0_2} + k_{0_3} n_{0_3} + k_{Ar} n_{Ar}}$$
(1)

where k_i is the rate coefficient of the quenching reaction by species i, and n_i is the number density of species i. Estimated densities of O, O₂, O₃ and Ar used in the calculation were taken from [26] and assumed to be 1×10^{16} cm⁻³, 2.5×10^{17} cm⁻³, 1×10^{14} cm⁻³ and 2.5×10^{19} cm⁻³, respectively. The obtained estimated lifetime of O₂($a^1\Delta_g$) is 13.1 ms, much longer than the estimated lifetimes of O₂($b^1\Sigma_g^+$) and O₂(v=1-4) which are 58.9 µs and 3.1 µs, respectively. Considering that it takes about 1-2 ms for the molecules or atoms to transit from the tip of the visible plasma plume to the substrate at nozzle-to-substrate distances of 5 to 8 mm, the possibility of the measurement of vibrationally excited species and O₂($b^1\Sigma_g^+$) at these distances can be discarded and the detected excited state of O₂ by MBMS is O₂($a^1\Delta_g$).

Table 1. Rate coefficients of the quenching reactions of $O_2(a^1\Delta_g)$, $O_2(b^1\Sigma_g^+)$ and $O_2(v=1-4)$, T_g is in unit K.

Reaction	Rate constant, $k \text{ (cm}^3 \text{ s}^{-1})$	Ref
$O_2(a^1\Delta_g) + O \rightarrow O_2 + O$	7.0×10 ⁻¹⁶	[27]

$O_2(a^1\Delta_g) + O_2 \rightarrow 2O_2$	$2.2 \times 10^{-18} (T_{\rm g}/300)^{0.8}$	[27]
$O_2(a^1\Delta_g) + O_3 \rightarrow 2O_2 + O$	$5.2 \times 10^{-11} \exp(-2840/T_{\rm g})$	[25]
$O_2(a^1\Delta_g) + Ar \rightarrow O_2 + Ar$	$3.0 \times 10^{-18} \exp(-200/T_{\rm g})$	[28]
$O_2(b^1\Sigma_g^+) + O \longrightarrow O_2(a^1\Delta_g) + O$	$8.0 \times 10^{-14} (T_{\rm g}/300)^{0.5}$	[25]
$O_2(b^1\Sigma_g^+) + O_2 \rightarrow O_2(a^1\Delta_g) + O_2$	$3.6 \times 10^{-17} (T_{\rm g}/300)^{0.5}$	[25]
$O_2(b^1\Sigma_g^+) + O_3 \rightarrow O_2(a^1\Delta_g) + O_3$	$7.33 \times 10^{-12} (T_g/300)^{0.5}$	[25]
$O_2(b^1\Sigma_g^+) + Ar \rightarrow O_2(a^1\Delta_g) + O_3$	6.0×10^{-16}	[28]
$O_2(v=1-4) + M \rightarrow O_2 + M$	$1.0 \times 10^{-14} (T_{\rm g}/300)^{0.5}$	[25]

3.2 Measurement approach I: plasma modulation

Fig. 4 presents a time-resolved measurement of $O_2(a^1\Delta_g)$ during a plasma modulation cycle with an ionizer electron energy of 11.5 eV and 12.5 eV for the 100 Hz plasma modulation. The increase in the O_2^+ signal during the plasma-on period can be divided into two parts a fast-rising signal and a slow rising signal due to accumulation in the ionizer. The latter confirms the accumulation of $O_2(a^1\Delta_g)$ inside the ionizer for 11.5 eV which is below the ionization energy of ground state O_2 . The build-up time constant of $O_2(a^1\Delta_g)$ inside the ionizer is estimated to be ~0.6 ms when considering the loss of $O_2(a^1\Delta_g)$ through openings in the ionizer and surface deactivation on the stainless steel surface of the housing with surface reaction probability $\gamma = (4-7) \times 10^{-3}$ [29]. This is similar to the value of 0.7 ms as obtained for ground state O_2 with the stame method. When using an ionizer electron energy of 12.5 eV, ground state O_2 can contribute to the O_2^+ signal during the plasma-on period. The same density of $O_2(a^1\Delta_g)$ measured by these two electron energies was compared and showed that the result obtained with 11.5 eV is 30% smaller than that obtained with 12.5 eV. This might be due to the fact that the ionization cross-section data of O_2 is less accurate for those low electron energies close to the ionization energy of $O_2(12.1 \text{ eV})$.

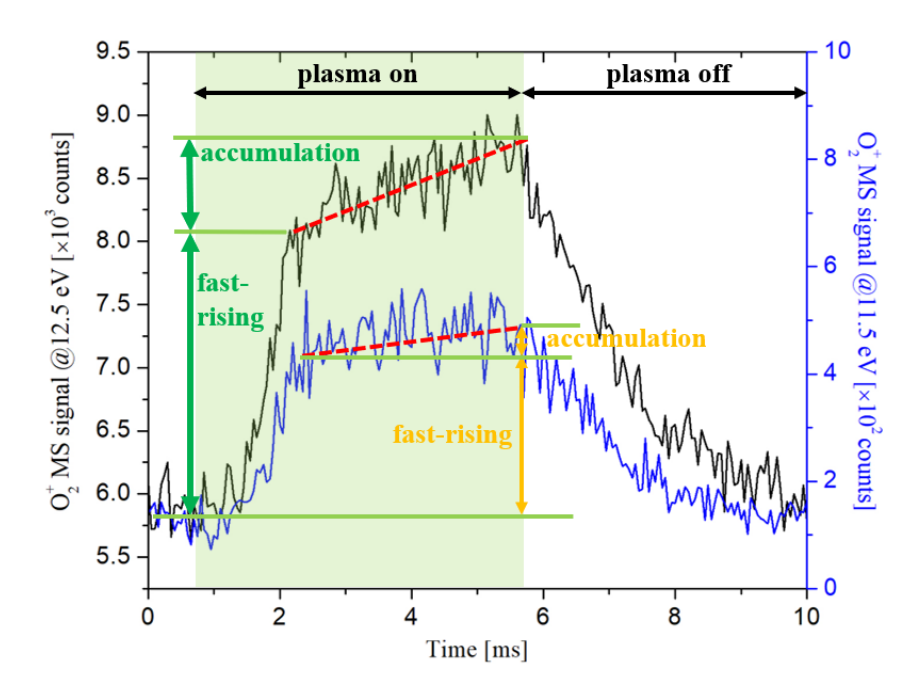


Figure 4. Time-resolved measurements of $O_2(a^1\Delta_g)$ during a plasma modulation cycle with an ionizer electron energy of 11.5 eV and 12.5 eV measured at a nozzle-substrate distance of 5 mm. The red dashed lines illustrate the linear increase in signals corresponding to the accumulation of $O_2(a^1\Delta_g)$ in the ionizer.

The absolute densities of $O_2(a^1\Delta_g)$ measured by the plasma modulation approach were calibrated using ground-state O_2 using the following expression:

$$\frac{n_{\text{O}_{2}(a^{1}\Delta_{\text{g}})}^{\text{on}}}{n_{\text{O}_{2}}^{\text{gas only}}} = \left(\frac{S_{12.5 \text{ eV}}^{\text{on,fast-rising}}}{\alpha \cdot S_{25 \text{ eV}}^{\text{gas only}}}\right) \cdot \left(\frac{\sigma_{25 \text{ eV}}^{\text{O}_{2} \to \text{O}_{2}^{+}}}{\sigma_{2(a^{1}\Delta_{\text{g}}) \to \text{O}_{2}^{+}}}\right), \tag{2}$$

where $S^{\text{on,fast-rising}}$ refers to the increase of MS signal for the fast-rising part during the plasma-on period. $n_{0_2}^{\text{gas only}}$ can be calculated from the known pressure and temperature of O_2 for the feed-gas-only case. The cross-section $\sigma^{O_2 \to O_2^+}$ was taken from the NIST database [30] and the cross-section of $\sigma^{O_2(a^1\Delta_g) \to O_2^+}$ is obtained by shifting the same cross-section by 0.98 eV. The electron energy (12.5 eV) of the ionizer used to detect $O_2(a^1\Delta_g)$ is above the ionization potential of ground-state O_2 to enhance the signals of $O_2(a^1\Delta_g)$ but the small contribution from O_2 ionization is accurately subtracted by $S_{12.5 \text{ eV}}^{\text{off}}$. The factor α , equal to the ratio of the beam signal to the total signal for the MBMS conditions used, is 0.25 as obtained by the second detection method with the

chopper, as explained below. This correction factor allows removing the non-beam contributions to the O_2^+ at 25 eV from background O_2 in the ionizer.

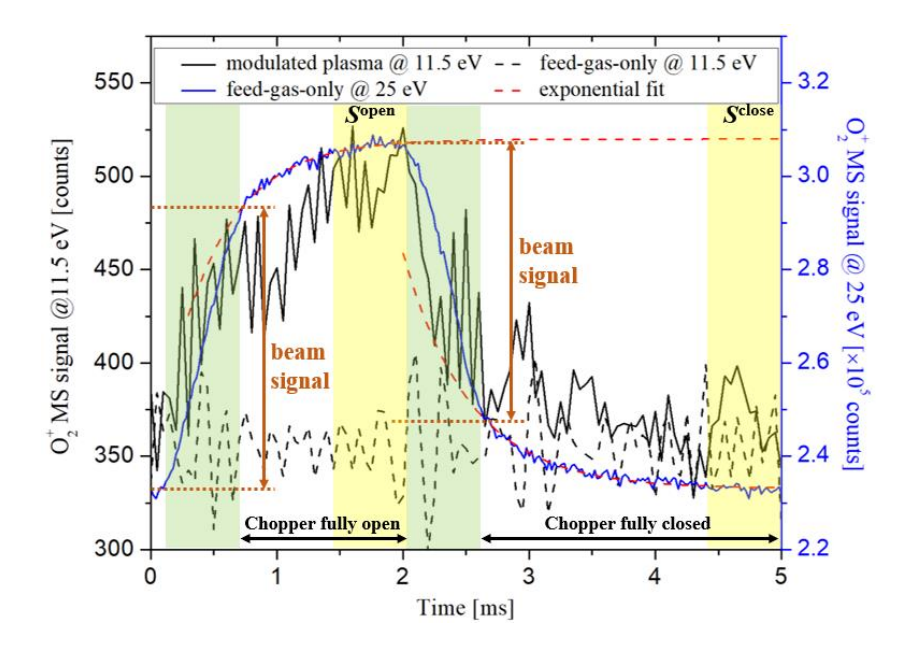


Figure 5. Time-resolved measurements of $O_2(a^1\Delta_g)$ and O_2 with the chopper (electron energies used to measure and calibrate $O_2(a^1\Delta_g)$ are 11.5 eV and 25 eV respectively). The plasma condition is the same as for Fig. 2 but measured at a nozzle-substrate distance of 8 mm. The red dashed line is an exponential fit of the signal increase and decrease after opening and closing of the chopper.

3.3 Measurement approach II: chopper modulation

Fig. 5 presents a time-resolved measurement of O_2^+ at an ionizer electron energy of 11.5 eV both for plasma and feed-gas-only cases with the chopper (200 Hz frequency) in use. The comparison of feed-gas-only with plasma clearly shows the contribution from $O_2(a^1\Delta_g)$ produced by the plasma, below the ionization potential of O_2 (12.1 eV). The good correspondence of the signals obtained for feed-gas-only and for the plasma case when the chopper is closed shows that we accurately subtract the background signal. Accumulations of O_2 and $O_2(a^1\Delta_g)$ in the ionizer during the chopper-fully-open and chopper-fully-closed periods are observed in the modulated O_2^+ signal in Fig. 5. This is a common problem caused by an ionizer only when measuring long-lived species because short-lived species typically recombine on walls of the ionizer and cannot be reflected back as background, as described in [31]. The background gas inside the ionizer is not being pumped out quickly enough compared with the chopper period, hence the background pressure inside the ionizer will change during the chopper modulation cycle. Furthermore, this pressure variation

inside the ionizer can be shown by the accumulation processes of MS signals, corresponding to the exponential increase and decrease in Fig. 5. As in [31], the fast increase and decrease of the signals immediately after the moments of chopper opening and closing correspond to the signal from the molecular beam, as marked in Fig. 5. The beam fraction α used in Eq. (2) can be also calculated by the beam signal and the exponential estimation of the "saturated" signal.

The difference of the MS signals for an ionization energy of 11.5 eV between the plasma-on and plasma-off cases in Fig. 5 is proportional to the $O_2(a^1\Delta_g)$ density and can be obtained by the following equation:

$$\frac{n_{\text{O}_{2}(a^{1}\Delta_{\text{g}})}^{\text{on}}}{n_{\text{O}_{2}}^{\text{gas only}}} = \left(\frac{\beta_{\text{O}_{2}(a^{1}\Delta_{\text{g}})} \cdot \left(S_{11.5 \text{ eV}}^{\text{open}} - S_{11.5 \text{ eV}}^{\text{close}}\right)}{\beta_{\text{O}_{2}} \cdot \left(S_{25 \text{ eV}}^{\text{open}} - S_{25 \text{ eV}}^{\text{close}}\right)}\right) \cdot \left(\frac{\sigma_{25 \text{ eV}}^{\text{O}_{2} \to \text{O}_{2}^{+}}}{\sigma_{11.5 \text{ eV}}^{\text{O}_{2}(a^{1}\Delta_{\text{g}}) \to \text{O}_{2}^{+}}}\right)$$
(3)

The factor β refers to the ratio of the beam signal to the sum of the beam signal and the accumulation signal and is equal to 0.8 for O₂. The signal of O₂($a^1\Delta_g$) was too noisy to obtain an accurate correction coefficient β , hence we assumed that $\beta_{O_2(a^1\Delta_g)}$ is identical to β_{O_2} because O₂($a^1\Delta_g$) has a similar behavior as O₂ inside the ionizer. The absolute densities obtained by the plasma modulation (9.7±1.5×10¹⁵ cm⁻³) and beam modulation (8.2±2.0×10¹⁵ cm⁻³) methods at a distance of 8 mm from the nozzle are in excellent agreement.

To validate the MBMS result against an independent technique, we also measured the absolute density of $O_2(a^1\Delta_g)$ produced by a micro-hollow dielectric barrier discharge source in air and compared it with the $O_2(a^1\Delta_g)$ density previously measured by IOES in [12] for the same plasma condition. The result of the IOES measurement $(7.5 \pm 0.8 \times 10^{14} \text{ cm}^{-3})$ corresponds within the experimental accuracy with the MBMS result: i.e. $9 \pm 4 \times 10^{14} \text{ cm}^{-3}$. Unfortunately, the measured $O_2(a^1\Delta_g)$ density by the MBMS in this case was close to the detection limit of the MBMS in spite of the signal being accumulated for about two hours. The comparison of the measured results obtained by MBMS and IOES nonetheless supports the accuracy of the new MBMS measurement.

3.4 Spatial distribution of $O_2(a^1\Delta_g)$

The MBMS has a unique advantage compared with previously reported optical diagnostic methods as it can easily provide a local density of the detected species near a substrate. Fig. 6 shows the absolute density of $O_2(a^1\Delta_g)$ as a function of the radial axis for three nozzle-to-substrate distances. The $O_2(a^1\Delta_g)$ densities decrease with increasing distance from the axis-of-symmetry of the APPJ. The gas convection induced by the gas flow through the jet makes the radial distribution of $O_2(a^1\Delta_g)$

more uniform for the nozzle-to-substrate distance of 11 mm compared with the radial density distribution at 5 mm. These radial profiles enable us to calculate the $O_2(a^1\Delta_g)$ fluxes impinging on the treated surface. As an example, the integrated flux of $O_2(a^1\Delta_g)$ at 5 mm over a circular area with a radius of 3 mm is 2.2×10^{19} s⁻¹, obtained by multiplying the species density with 1/4 of its thermal velocity.

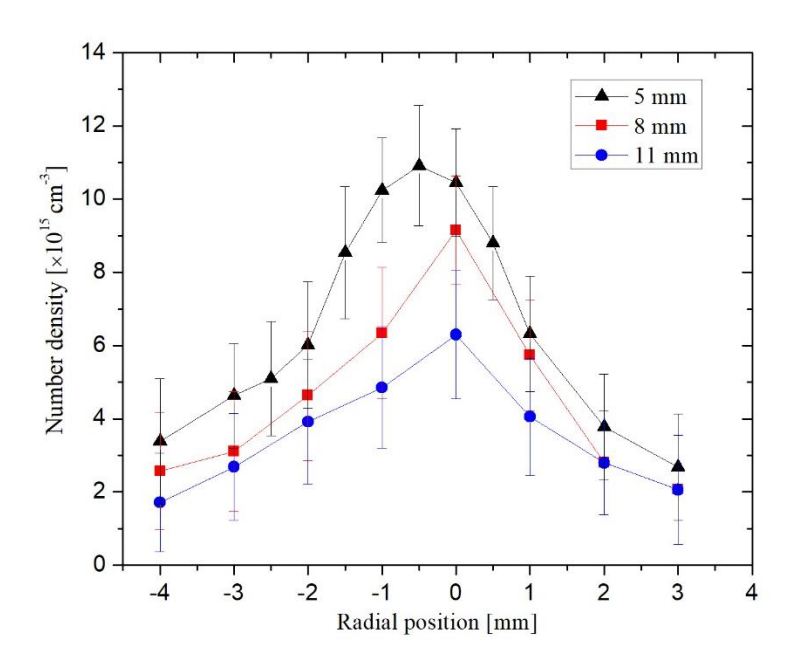


Figure 6. Absolute densities of $O_2(a^1\Delta_g)$ as a function of radial distance for three different nozzle-to-substrate distances.

The absolute densities for O and $O_2(a^1\Delta_g)$ in the center position of the APPJ as a function of the nozzle-to-substrate distance are shown in Fig. 7. The atomic oxygen was measured as described in detail in [21]. A pseudo-plug flow model as described in [21],[24],[28] was used to compare with the experimental results of the MBMS. The simulated and experimentally obtained absolute densities of O and $O_2(a^1\Delta_g)$ in the afterglow region of the APPJ are in good agreement. The results also show the dominance of $O_2(a^1\Delta_g)$ over O in the jet afterglow suggesting its importance in the effluent reaction kinetics. In addition, the high gas-phase concentration of $O_2(a^1\Delta_g)$ in the RF jet is consistent with the previously reported dominance of $O_2(a^1\Delta_g)$ in the inactivation of virus by the same plasma jet although operated under slightly different conditions [32].

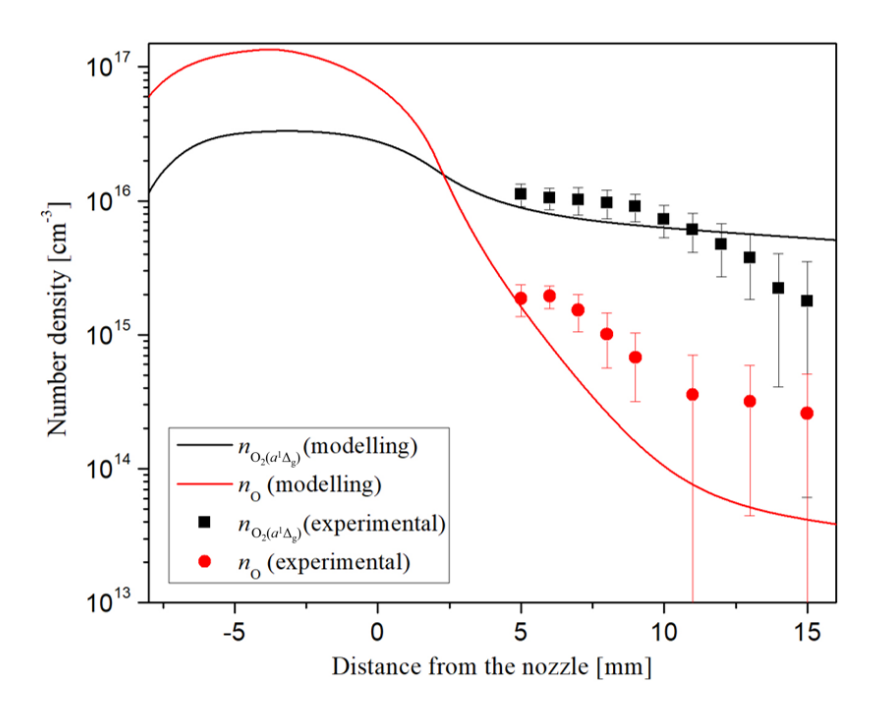


Figure 7. Absolute densities of O and $O_2(a^1\Delta_g)$ in the center of APPJ as a function of nozzle-to-substrate distance

4. Conclusion

In this manuscript, the axial and radial absolute density profiles of $O_2(a^1\Delta_g)$ were measured in an APPJ using MBMS. The results illustrate the advantage of MBMS enabling the direct evaluation of $O_2(a^1\Delta_g)$ impinging on substrates. The diagnostic technique might be of significant value for evaluating the role of $O_2(a^1\Delta_g)$ in plasma-surface interactions in the context of plasma-medical therapies and plasma-catalysis.

Acknowledgment

This work was supported by the National Science Foundation (CBET 1703439) and US Department of Energy, Office of Fusion Energy Sciences (DESC0001939). The authors sincerely thank Prof. M Kushner (U of Michigan) for providing the GLOBALKIN code. The authors acknowledge the Minnesota Supercomputing Institute (MSI) at the University of Minnesota in providing resources that contributed to the results reported in this paper.

Reference

[1] Ionin, A. A.; Kochetov, I. V; Napartovich, A. P.; Yuryshev, N. N. Physics and Engineering of Singlet Delta Oxygen Production in Low-Temperature Plasma. *J. Phys. D. Appl. Phys.* **2007**, *40* (2), R25–R61.

- [2] Weishaupt, K. R.; Gomer, C. J.; Dougherty, T. J. Identification of Singlet Oxygen as the Cytotoxic Agent in Photoinactivation of a Murine Tumor. *Cancer Res.* **1976**, *36* (7 PT 1), 2326–2329.
- [3] Bauer, G.; Graves, D. B. Mechanisms of Selective Antitumor Action of Cold Atmospheric Plasma-Derived Reactive Oxygen and Nitrogen Species. *Plasma Process. Polym.* **2016**, *13* (12), 1157–1178.
- [4] Smirnov, V. V; Stelmakh, O. M.; Fabelinsky, V. I.; Kozlov, D. N.; Starik, A. M.; Titova, N. S. On the Influence of Electronically Excited Oxygen Molecules on Combustion of Hydrogen–Oxygen Mixture. J. Phys. D. Appl. Phys. 2008, 41 (19), 192001.
- [5] Lebedev, A. V.; Deminsky, M. A.; Zaitzevsky, A. V.; Potapkin, B. V. Effect of $O_2(a^1\Delta_g)$ on the Low-Temperature Mechanism of CH₄ Oxidation. *Combust. Flame* **2013**, *160* (3), 530–538.
- [6] Whitehead, J. C. Plasma–Catalysis: The Known Knowns, the Known Unknowns and the Unknown Unknowns. *J. Phys. D. Appl. Phys.* **2016**, *49* (24), 243001.
- [7] Földes, T.; Čermák, P.; Macko, M.; Veis, P.; Macko, P. Cavity Ring-down Spectroscopy of Singlet Oxygen Generated in Microwave Plasma. *Chem. Phys. Lett.* **2009**, *467* (4–6), 233–236.
- [8] Williams, S.; Gupta, M.; Owano, T.; Baer, D. S.; O'Keefe, A.; Yarkony, D. R.; Matsika, S. Quantitative Detection of Singlet O₂ by Cavity-Enhanced Absorption. *Opt. Lett.* **2004**, *29* (10), 1066.
- [9] Wu, Y.; Zhang, Z.; Ombrello, T. M. Spatially Resolved Measurement of Singlet Delta Oxygen by Radar Resonance-Enhanced Multiphoton Ionization. *Opt. Lett.* **2013**, *38* (13), 2286.
- [10] Sousa, J. S.; Bauville, G.; Puech, V. Arrays of Microplasmas for the Controlled Production of Tunable High Fluxes of Reactive Oxygen Species at Atmospheric Pressure. *Plasma Sources Sci. Technol.* **2013**, *22* (3), 035012.
- [11] Sousa, J. S.; Puech, V. Diagnostics of Reactive Oxygen Species Produced by Microplasmas. *J. Phys. D. Appl. Phys.* **2013**, *46* (46), 464005.
- [12] Nayak, G.; Sousa, J. S.; Bruggeman, P. J. Singlet Delta Oxygen Production in a 2D Micro-Discharge Array in Air: Effect of Gas Residence Time and Discharge Power. *J. Phys. D.*

- Appl. Phys. 2017, 50 (10), 105205.
- [13] Sousa, J. S.; Niemi, K.; Cox, L. J.; Th Algwari, Q.; Gans, T. Cold Atmospheric Pressure Plasma Jets as Sources of Singlet Delta Oxygen for Biomedical Applications. *J. Appl. Phys* **2011**, *109*, 123302.
- [14] Inoue, Y.; Ono, R. Measurement of Singlet Delta Oxygen in an Atmospheric-Pressure Helium–Oxygen Plasma Jet. *J. Phys. D. Appl. Phys.* **2017**, *50* (21), 214001.
- [15] Willems, G.; Benedikt, J.; von Keudell, A. Absolutely Calibrated Mass Spectrometry Measurement of Reactive and Stable Plasma Chemistry Products in the Effluent of a He/H 2 O Atmospheric Plasma. *J. Phys. D. Appl. Phys.* **2017**, *50* (33), 335204.
- [16] Große-Kreul, S.; Hübner, S.; Schneider, S.; Ellerweg, D.; von Keudell, A.; Matejčík, S.; Benedikt, J. Mass Spectrometry of Atmospheric Pressure Plasmas. *Plasma Sources Sci. Technol.* **2015**, *24* (4), 044008.
- [17] Krähling, T.; Ellerweg, D.; Benedikt, J. The Influence of the Ionizer Geometry on the Absolute Density Calibration of Reactive Neutral Species in a Molecular Beam Mass Spectrometry. *Rev. Sci. Instrum.* **2012**, *83* (4), 045114.
- [18] Willems, G.; Golda, J.; Ellerweg, D.; Benedikt, J.; von Keudell, A.; Knake, N.; Schulz-von der Gathen, V. Corrigendum: Characterization of the Effluent of a He/O₂ Micro-Scaled Atmospheric Pressure Plasma Jet by Quantitative Molecular Beam Mass Spectrometry (2010 New J. Phys. 12 013021). New J. Phys. 2019, 21 (5), 059501.
- [19] Schneider, S.; Dünnbier, M.; Hübner, S.; Reuter, S.; Benedikt, J. Atomic Nitrogen: A Parameter Study of a Micro-Scale Atmospheric Pressure Plasma Jet by Means of Molecular Beam Mass Spectrometry. J. Phys. D. Appl. Phys. 2014, 47 (50), 505203.
- [20] van Ham, B. T. J.; Hofmann, S.; Brandenburg, R.; Bruggeman, P. J. In Situ Absolute Air, O 3 and NO Densities in the Effluent of a Cold RF Argon Atmospheric Pressure Plasma Jet Obtained by Molecular Beam Mass Spectrometry. J. Phys. D. Appl. Phys. 2014, 47 (22), 224013.
- [21] Jiang, J.; Luo, Y.; Moldgy, A.; Aranda Gonzalvo, Y.; Bruggeman, P. J. Absolute Spatially and Time-Resolved O, O₃, and Air Densities in the Effluent of a Modulated RF-Driven Atmospheric Pressure Plasma Jet Obtained by Molecular Beam Mass Spectrometry. *Plasma Process. Polym.* **2019**, e1900163.

- [22] Bruggeman, P.; Iza, F.; Lauwers, D.; Gonzalvo, Y. A. Mass Spectrometry Study of Positive and Negative Ions in a Capacitively Coupled Atmospheric Pressure RF Excited Glow Discharge in He–Water Mixtures. *J. Phys. D. Appl. Phys.* **2009**, *43* (1), 12003.
- [23] Hofmann, S.; Van Gessel, A. F. H.; Verreycken, T.; Bruggeman, P. Power Dissipation, Gas Temperatures and Electron Densities of Cold Atmospheric Pressure Helium and Argon RF Plasma Jets. *Plasma Sources Sci. Technol.* 2011, 20 (6), 065010.
- [24] Zhang, S.; van Gaens, W.; van Gessel, B.; Hofmann, S.; van Veldhuizen, E.; Bogaerts, A.; Bruggeman, P. Spatially Resolved Ozone Densities and Gas Temperatures in a Time Modulated RF Driven Atmospheric Pressure Plasma Jet: An Analysis of the Production and Destruction Mechanisms. J. Phys. D. Appl. Phys. 2013, 46 (20), 205202.
- [25] Liu, D.-X.; Rong, M.-Z.; Wang, X.-H.; Iza, F.; Kong, M. G.; Bruggeman, P. Main Species and Physicochemical Processes in Cold Atmospheric-Pressure He + O₂ Plasmas. *Plasma Process. Polym.* **2010**, 7 (9–10), 846–865.
- [26] Wende, K.; Williams, P.; Dalluge, J.; Van Gaens, W.; Aboubakr, H.; Bischof, J.; von Woedtke, T.; Goyal, S. M.; Weltmann, K.-D.; Bogaerts, A.; et al. Identification of the Biologically Active Liquid Chemistry Induced by a Nonthermal Atmospheric Pressure Plasma Jet. *Biointerphases* 2015, 10 (2), 029518.
- [27] Gordillo-Vázquez, F. J. Air Plasma Kinetics under the Influence of Sprites. *J. Phys. D. Appl. Phys.* **2008**, *41* (23), 234016.
- [28] Gaens, W. Van; Bogaerts, A. Kinetic Modelling for an Atmospheric Pressure Argon Plasma Jet in Humid Air. *J. Phys. D. Appl. Phys.* **2013**, *46* (27), 275201.
- [29] Sharpless, R. L.; Slanger, T. G. Surface Chemistry of Metastable Oxygen. II. Destruction of O 2 (a 1 Δ G). *J. Chem. Phys.* **1989**, *91* (12), 7947–7950.
- [30] Kim, Y.-K.; Irikura, K. K.; Rudd, M. E.; Ali, M. A.; Stone, P. M.; Chang, J.; Coursey, J. S.; Dragoset, R. A.; Kishore, A. R.; Olsen, K. J.; et al. Electron-impact cross sections for ionization and excitation. NIST Standard Reference Database. 2010; 107.
- [31] Cunge, G.; Bodart, P.; Brihoum, M.; Boulard, F.; Chevolleau, T.; Sadeghi, N. Measurement of Free Radical Kinetics in Pulsed Plasmas by UV and VUV Absorption Spectroscopy and by Modulated Beam Mass Spectrometry. *Plasma Sources Sci. Technol.* **2012**, *21* (2), 024006.

[32] Aboubakr, H. A.; Gangal, U.; Youssef, M. M.; Goyal, S. M.; Bruggeman, P. J. Inactivation of Virus in Solution by Cold Atmospheric Pressure Plasma: Identification of Chemical Inactivation Pathways. *J. Phys. D. Appl. Phys.* **2016**, *49* (20), 204001.